Strong embedded discontinuities for simulating fracture in quasi-brittle materials

J. Alfaiate[1], G. N. Wells[2] & L. J. Sluys[2]
[1]*Instituto Superior Técnico, Lisboa, Portugal*
[2]*Koiter Institute Delft / Delft University of Technology, Delft, The Netherlands*

In this paper embedded strong discontinuities are used to model discrete cracking in materials like concrete. In the approach followed a discontinuous displacement field is considered and the deformation is localized at a surface of zero width. Both a damage law and a plasticity law are adopted to describe the constitutive relation between tractions and displacement jumps at the discontinuity surface. An algorithm is introduced to enforce the continuity of the crack path, permitting a clear identification of the discontinuities in the mesh. Both mode I and mixed mode cracking have been considered and the importance of the shear tractions on the global behaviour of a structure is assessed. With the formulation adopted it is concluded that: i) realistic crack patterns are obtained, similar to those found in experiments and ii) the dissipation of energy can be objectively found irrespective of the mesh that is used.

1 INTRODUCTION

The finite element method has been used in the past to simulate strain-softening in the continuum. Considerable research has been done in order to overcome the mesh dependence found with non-regularized models. Non-local and gradient models are representatives of this work. In these formulations damage occurs within bands of finite width, set by an internal length scale parameter, which is considered a material property. As a consequence, strong discontinuities, which correspond to localized surfaces or cracks, can not be explicitly represented in these models. On the other hand, the discrete approach has been used to simulate localized softening through the use of a cohesive formulation. This formulation has the advantage of being independent of the mesh with respect to the dissipation of energy if the crack path is aligned with the mesh. Since discontinuities are modelled by interfaces inserted along element boundaries, the mesh has to be either aligned *a priori* or during a calculation. The general case for which the crack path is not known presents an additional difficulty for this formulation which has been dealt with in two ways: i) the finite element mesh is redefined in each step in order to align the interfaces with the directions of the crack path predicted by the model (Carpinteri et al. 1989); ii) the properties of the correct crack path are projected on the finite element mesh in such a way that

both the energy dissipation and the crack patterns are accurately predicted (Alfaiate et al. 1997). Although both approximations have been successful in reproducing the localized softening behaviour of quasi-brittle materials like concrete, numerical difficulties are encountered, such as: i) the remeshing procedures lead to distorted meshes and an increased bandwidth of the stiffness matrix; ii) a large number of interfaces have to be present in the finite element mesh (and consequently a large number of degrees of freedom) from the beginning of the calculations if the latter approach is adopted since, in this case, no remeshing procedures are considered. A more promising method seems to consist of a mixed formulation in which the dissipation of energy can be objectively found with respect to the mesh, whereas continuum elements can still be used to reproduce softening. Such a formulation is presented here in which discrete cracking is modelled through the consideration of strong discontinuities embedded in finite elements. Several examples of this formulation can be found in recent literature where two different approaches have being followed: i) a strong discontinuity is approximated as a limit case of a weak discontinuity through the definition of a bandwidth parameter which tends to zero (Oliver et al. 1999) and ii) a real strong discontinuity is simulated considering a discontinuous displacement field (Wells and Sluys 2001). In this paper the latter concept is redressed. In particular, special at-

tention will be paid to: i) the enforcement of the continuity of the crack path, for which a new algorithm is introduced and ii) the effect of shear tractions at the discontinuities on the global structural behaviour. Examples of mode I and mixed mode cracking evolution are presented. The effect of shear stresses on the global structural response of a single-edge notched (SEN) beam is analyzed with different constitutive models. The results are obtained with structured and unstructured meshes and compare favorably with the experimental data.

2 KINEMATICS OF A STRONG DISCONTINUITY

A strong discontinuity is characterized by a jump on the displacement field, localized at a surface. Consider a domain Ω, with boundary $\partial\Omega$ where a discontinuity surface Γ_d is supposed to exist. The displacement field contains a regular part on Ω, $\hat{\mathbf{u}}$, and an irregular part corresponding to the displacement jump, $[\![\mathbf{u}]\!]$, localized at the discontinuity surface Γ_d:

$$\mathbf{u}(\mathbf{x}) = \hat{\mathbf{u}}(\mathbf{x}) + \mathcal{H}_{\Gamma_d}[\![\mathbf{u}(\mathbf{x})]\!] \tag{1}$$

where $\mathcal{H}_{\Gamma_d}$ is the Heaviside function at the discontinuity Γ_d,

$$\mathcal{H}_{\Gamma_d} = \begin{cases} 1 & \text{if } \mathbf{x} \in \Omega^+ \\ 0 & \text{otherwise} \end{cases} \tag{2}$$

The corresponding infinitesimal strain field is:

$$\begin{aligned} \boldsymbol{\varepsilon} = \boldsymbol{\nabla}^{\text{s}}\mathbf{u} \quad &= \boldsymbol{\nabla}^{\text{s}}\hat{\mathbf{u}} + \mathcal{H}_{\Gamma_d}\left(\boldsymbol{\nabla}^{\text{s}}[\![\mathbf{u}]\!]\right) + \left(\boldsymbol{\nabla}\mathcal{H}_{\Gamma_d} \otimes [\![\mathbf{u}]\!]\right)^{\text{s}} \\ &= \underbrace{\boldsymbol{\nabla}^{\text{s}}\hat{\mathbf{u}} + \mathcal{H}_{\Gamma_d}\left(\boldsymbol{\nabla}^{\text{s}}[\![\mathbf{u}]\!]\right)}_{\text{bounded}} + \underbrace{\delta_{\Gamma_d}\left([\![\mathbf{u}]\!] \otimes \mathbf{n}\right)^{\text{s}}}_{\text{unbounded}} \end{aligned} \tag{3}$$

where $(\cdot)^{\text{s}}$ refers to the symmetric part of $(\cdot)$, and δ_{Γ_d} is the Dirac delta-function along surface Γ_d.

Here, similar to the work presented in (Armero and Garikipati 1996; Wells and Sluys 2001), no regularization is performed on the irregular part of the strain field.

3 MATERIAL MODELS

The bulk behaviour is modeled by means of a linear-elastic constitutive relation. Two different models are used for the discontinuity: a damage law and a plasticity law. It is assumed that cracking always initiates according to a mode I criterion, when the maximum principal stress reaches the tensile strength of the material f_t. Crack evolution is modelled according to mixed mode fracture allowing shear stresses to develop along the crack faces of the discontinuity, due to aggregate interlocking and/or shear fracture.

3.1 DAMAGE MODEL

The model considered in this section was first introduced in (Wells and Sluys 2001) for three dimen-

sional problems. Here, a two dimensional version of the model is presented. A loading function is defined as:

$$f(w_n, \kappa) = w_n - \kappa \tag{4}$$

where w_n is the normal component to the crack surface, of the displacement jump at the discontinuity surface Γ_d. The internal variable κ is taken as the maximum normal relative displacement reached ($\kappa = \max(w_n), \dot{\kappa} \geq 0$). Direction $\mathbf{n}$ is aligned with the direction of the maximum principal stress. If $f > 0$ loading takes place ($\dot{\kappa} > 0$), whereas if $f < 0$ closing of the crack occurs and damage does not grow ($\dot{\kappa} = 0$). An exponential softening law is adopted for the relation between the normal traction component t_n and the normal relative displacement between the crack faces (normal jump), given by

$$t_n = f_{t0}\exp\left(-\frac{f_{t0}}{G_F}\kappa\right) \tag{5}$$

where G_F is the fracture energy and f_{t0} is the initial tensile strength of the material. The shear traction component t_s is related to the sliding relative displacement along crack faces (shear jump w_s) according to a relation independent of eq. (5), given by:

$$t_s = D_{s0}\exp\left(h_s\kappa\right)w_s, \tag{6}$$

where D_{s0} is the initial shear stiffness at crack initiation, h_s is given by

$$h_s = \ln\left(D_{s\kappa}/D_{s0}\right) \tag{7}$$

and $D_{s\kappa}$ is the shear stiffness which is adopted for an advanced state of damage ($\kappa\,0$). Since relations (5) and (6) are independent, the model introduces non-isotropic damage in the traction space; as a consequence, it is possible to enforce mode I crack evolution since the shear tractions can be made equal to zero simply by imposing $D_{s0} = 0$. The incremental constitutive relation in matrix form is given by,

$$\begin{Bmatrix} \dot{t}_n \\ \dot{t}_s \end{Bmatrix} = \begin{bmatrix} -\frac{f_{t0}^2}{G_F}\exp\left(-\frac{f_{t0}}{G_F}\kappa\right) & 0 \\ h_s D_{s0}\exp\left(h_s\kappa\right)w_s & D_{s0}\exp\left(h_s\kappa\right) \end{bmatrix} \begin{Bmatrix} \dot{w}_n \\ \dot{w}_s \end{Bmatrix}. \tag{8}$$

The secant stiffness matrix is used for unloading, which is given by

$$\mathbf{D}_{unloading} = \begin{bmatrix} \frac{f_{t0}}{\kappa}\exp\left(-\frac{f_{t0}}{G_F}\kappa\right) & 0 \\ 0 & D_{s0}\exp\left(h_s\kappa\right) \end{bmatrix}. \tag{9}$$

If a crack fully closes, i.e., $w_n = 0$, a very large value for the *elastic* stiffness is assumed in order to prevent overlapping of the crack faces.
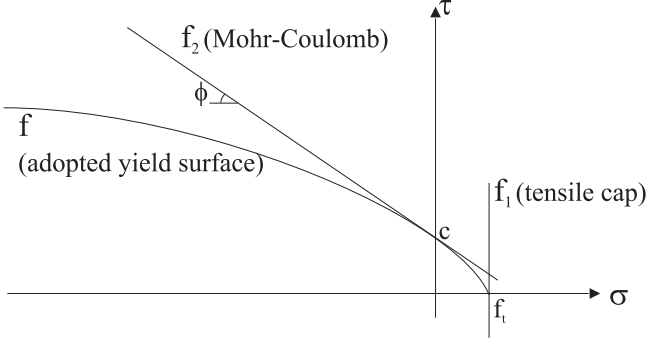
2

Figure 1: Adopted yield surface f, the tensile cap f_1 and Mohr-Coulomb friction law f_2.

3.2 PLASTICITY MODEL

In this model, a limit surface is defined in the traction space $\{t_n, t_s\}$ such that both tensile mode I cracking and a modified friction Coulomb envelope are taken into account. In fig. 1 the adopted yield surface is shown. It is given by

$$f = t_s^2 - f_t - \frac{f_t^2 + 2c\tan\phi f_t - c^2}{f_t^2} t_n^2$$
$$- c^2 \left(1 + \tan^2\phi\right) + (t_n + \tan\phi c)^2 = 0 \quad (10)$$

where ϕ is the internal friction angle, c is the cohesion and f_t is the tensile strength. In fig. 1, two other limit surfaces are also presented which envelope the surface f adopted. The first, denoted as f_1, is a tensile cap and the second envelope surface f_2 is the Mohr-Coulomb friction law. Two energies associated with fracture are defined as material properties: the fracture energy G_F and the energy G_F^{II}, defined in mode II or shear cracking, given by the area below the shear stress-sliding displacement curve obtained in the absence of a normal confining load. Thus, in G_F^{II} both the dissipation of energy due to friction (aggregate interlocking) and due to shear fracture are taken into account. Both the tensile strength f_t and the cohesion c are functions of an internal scalar variable κ according to the exponential laws:

$$f_t = f_{t0} \exp\left(-\frac{f_{t0}}{G_F}\kappa\right) \quad (11)$$

$$c = c_0 \exp\left(-\frac{c_0}{G_F^{II}}\kappa_s\right) \quad (12)$$

where f_{t0} is the initial tensile strength and c_0 is the initial cohesion value (for $\kappa = 0$). An isotropic softening criterion is adopted such that:

$$\kappa = \kappa_n = w_n^p + \frac{c_0 G_F}{f_{t0} G_F^{II}} w_s^p \quad (13)$$

$$\kappa_s = \kappa_n \frac{f_{t0} G_F^{II}}{c_0 G_F} \quad (14)$$

where w_n^p and w_s^p are equal to the plastic normal and sliding displacement jumps, respectively. Generally, a non-associative flow rule is adopted, such that

$$\dot{\mathbf{w}}^p = \dot{\lambda}\frac{\partial g}{\partial \mathbf{t}}, \quad (15)$$

where λ is the plastic multiplier. The direction of plastic flow is normal to a plastic potential assumed to be a function of the tractions, $g = g(\mathbf{t})$. Let ψ be the dilatancy angle which is considered fixed if $t_n < 0$. In the compressive zone of the traction space, g is given by

$$g = |t_s| + t_n \tan\psi - c, \quad (16)$$

whereas, for the particular case of pure mode I cracking ($t_s = 0$), the flow rule becomes associative and g is given by

$$g = f_1 = t_n - f_t. \quad (17)$$

The derivatives of the plastic potential with respect to the traction components vary continuously between tensile and compressive tractions in mixed mode fracture, assuring a smooth transition for the direction of plastic flow (Alfaiate et al. 2001). A backward-Euler return mapping algorithm is used and the consistent tangent traction-displacement jump relationship, in matrix form, is given by:

$$\dot{\mathbf{t}} = \left[\mathbf{H} - \frac{\mathbf{H}\frac{\partial g}{\partial \mathbf{t}}\frac{\partial f}{\partial \mathbf{t}}^T\mathbf{H}}{\frac{\partial f}{\partial \mathbf{t}}^T\mathbf{H}\frac{\partial g}{\partial \mathbf{t}} - h}\right]\dot{\mathbf{w}}, \quad (18)$$

where h is the plastic modulus and

$$\mathbf{H} = \left[\mathbf{I} + \Delta\lambda\mathbf{D}_{\Gamma_d}^{el}\frac{\partial^2 g}{\partial \mathbf{t}^2}\right]^{-1}\mathbf{D}_{\Gamma_d}^{el}. \quad (19)$$

At crack initiation, the elastic part has to be assumed such that, for brittle cracking and according to Rankine's criterion, the following conditions are met:

$$
\begin{aligned}
t_n &= \sigma_I = f_t \\
t_s &= 0 \\
w_n^{el} &= \frac{f_t}{D_{nn}^{el}} \\
w_n^p &= 0 \\
w_s^{el} &= w_s^p = 0.
\end{aligned} \quad (20)
$$

Similarly to the damage model, a penalty formulation is used to prevent overlapping of crack faces. As a consequence, the diagonal elastic stiffness components D_{nn}^{el} and D_{ss}^{el} are given very high values.

4 NUMERICAL IMPLEMENTATION

The finite element discretisation is based on constant strain triangles. For each element, crossed by a discontinuity, an internal node is defined where the localized constitutive relation is applied. The two degrees of freedom of this internal node correspond to the jump displacement components at the discontinuity. As a consequence, the jump displacement field is assumed to be of the same order as the strain field, i.e., a constant displacement jump is assumed at the discontinuity over the entire element. This leads to non-continuous displacement jumps at the discontinuities across the boundary of the elements. However, since the tractions at the discontinuity are directly related to the correspondent displacement field (see section 3), the lack of continuity of the traction field across element boundaries is in agreement with the lack of continuity of the stress field across the same boundaries. Incrementally, the traction continuity condition is given by:

$$-\frac{l_d}{\Omega}\int_\Omega \dot{\boldsymbol{\sigma}}\cdot\mathbf{n}d\Omega + \int_{\Gamma_d}\dot{\mathbf{t}}d\Gamma = \mathbf{0} \qquad (21)$$

where $\dot{\mathbf{t}}$ is the incremental traction vector obtained at the discontinuity Γ_d, $\mathbf{n}$ is the normal to the discontinuity, $\dot{\boldsymbol{\sigma}}$ is the incremental stress tensor and l_d is the length of the discontinuity Γ_d. Equation (21) is equivalent to:

$$\frac{1}{l_d}\int_{\Gamma_d}\dot{\mathbf{t}}d\Gamma - \frac{1}{\Omega}\int_\Omega \dot{\boldsymbol{\sigma}}\cdot\mathbf{n}d\Omega = \mathbf{0} \qquad (22)$$

which shows that traction continuity is enforced in an averaged sense. However, as previously stated, since constant stresses and tractions are assumed over both the length l_d and the domain Ω, equations (21) and (22) also enforce traction continuity locally, within an element. Moreover, it can also be seen from equation (22) that the formulation does not depend upon the length of the discontinuities l_d. Note however, that the relative position of the discontinuities with respect to the elements is taken into account due to the enforcement of crack path continuity, as shown below.

Each time a new crack is initiated a check is carried out for the existence of crack tips in the neighbourhood, on the element sides. The following cases are considered (Alfaiate et al. 2001):

1. if there is no crack tip at the element sides evaluate the position of the new crack tips (two) such that the crack path passes through the centroid of the element (see fig. 2 a);

2. if there is one crack tip at one element side, evaluate the position of the new crack tip on the opposite element boundary (see fig. 2 b);
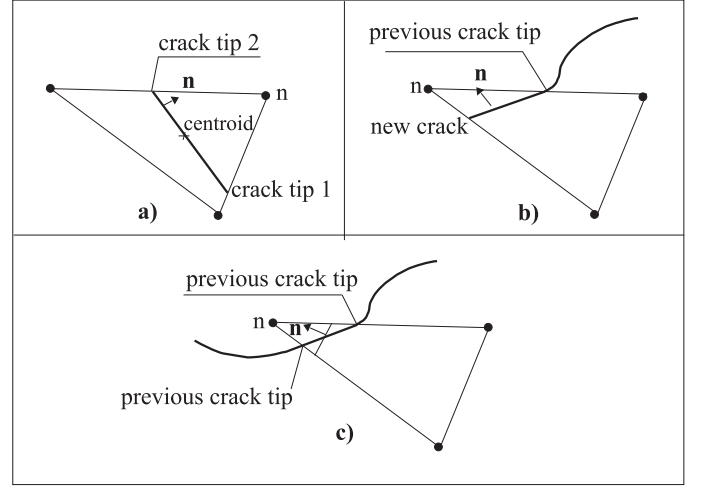

Figure 2: Enforcing crack path continuity.

3. if there are two crack tips connect them to one another (see fig. 2 c), but preserve the direction of the normal evaluated for future calculations.

For each crack, the information regarding the coordinates of the crack tips as well as the nodes delimiting the side of the element where it lies is stored: (i) first temporarily during the convergence procedure and (ii) definitively only when a converged solution is found. This is due to the fact that, during the iterative process, it may happen that a fictitious crack which was initiated at a previous iteration is no longer active at the present iteration and has to be removed from the active set together with all hypothetical discontinuities ahead of it. Finally, due to jumps in the approximated stress field, it may happen that new cracks do not always tend to initiate at existing crack tips. In order to prevent such improbable situation, new crack paths are allowed to initiate only outside the neighbourhood of existing crack tips. This neighbourhood is defined by a radius of influence centred at the crack tip. A value related to the aggregate size is proposed since it seems physically realistic. In fact, it is expected that, at least, one aggregate must lie in the neighbourhood of an existing crack tip, preventing new cracks to initiate at this vicinity. In the analysis performed this radius is taken equal to four times the element size, which is of the order of the maximum aggregate size.

For each finite element, the principle of virtual work leads to:

$$\int_{\Omega_e}\mathbf{B}^T\boldsymbol{\sigma}d\Omega = \mathbf{f}^{ext} \qquad (23)$$

where $\mathbf{B}^T$ contains the derivatives of the shape functions and $\mathbf{f}^{ext}$ is the nodal force vector. For updating the stresses, the kinematically constructed interpolation matrix $\mathbf{G}$ is used, such that (Wells and Sluys 2001):

$$\dot{\boldsymbol{\sigma}} = \mathbf{D}(\mathbf{B} + \mathbf{G}\dot{\mathbf{w}}) \qquad (24)$$

where, for a plane stress or strain state, matrix $\mathbf{G}$ is given by:

$$\mathbf{G} = \begin{bmatrix} \delta_{\Gamma_d} n_1 - \frac{\partial \varphi(\mathbf{x})}{\partial x_1} & 0 \\ 0 & \delta_{\Gamma_d} n_2 - \frac{\partial \varphi(\mathbf{x})}{\partial x_2} \\ 0 & 0 \\ \delta_{\Gamma_d} n_2 - \frac{\partial \varphi(\mathbf{x})}{\partial x_2} & \delta_{\Gamma_d} n_1 - \frac{\partial \varphi(\mathbf{x})}{\partial x_1} \end{bmatrix}. \qquad (25)$$

In eq. (25), $\varphi(\mathbf{x})$ is the shape function corresponding to node n towards which the normal at the discontinuity is pointed at (see fig. 2). Thus, depending on the relative position of the discontinuity inside the element, a specific node n is chosen leading to a different $\mathbf{G}$ matrix. Since the enforcement of crack path continuity influences this relative position, it also influences matrix $\mathbf{G}$ and the stress update.

Taking into account the traction continuity condition, and the principle of virtual work, the weak formulation leads, after linearisation, to a set of equations in which the incremental jumps $d\mathbf{w}$ can be solved by static condensation. In the end, it is possible to write (Wells and Sluys 2001):

$$\mathbf{K}_{con} d\mathbf{a} = d\mathbf{f}_{ext} \qquad (26)$$

where $\mathbf{K}_{con}$ is the condensed incremental stiffness matrix and $d\mathbf{a}$ are the incremental nodal displacements. According to (26) only the standard degrees of freedom are taken into account when solving the system of equations.

5 NUMERICAL RESULTS

In this section, the numerical results obtained for two different tests are presented: a tension test and a single-edge notched beam. Both tests are examples of quasi-brittle mode I and mixed mode fracture.

5.1 TENSILE TESTS

The tension tests have been performed for double-edge notched specimens as shown in fig. 3. Experimental tests were performed in mortar and 8mm concrete specimens with this geometry (Shi et al. 2000). The off-set values adopted experimentally were 0, 5, 10 and 15 mm, symmetric with respect to the horizontal centre axis of the specimen. The specimen was glued directly to the loading platens.

In the simulations presented here, only the 8 mm concrete and notch off-set values of 5mm and 15 mm are considered. The bottom edge is fixed and the top edge is fixed in the horizontal direction in order to simulate the gluing to the loading platens. A vertical displacement is imposed at the top edge of the specimen (see fig.4). The load displacement responses, both experimental and numerical, relate the average
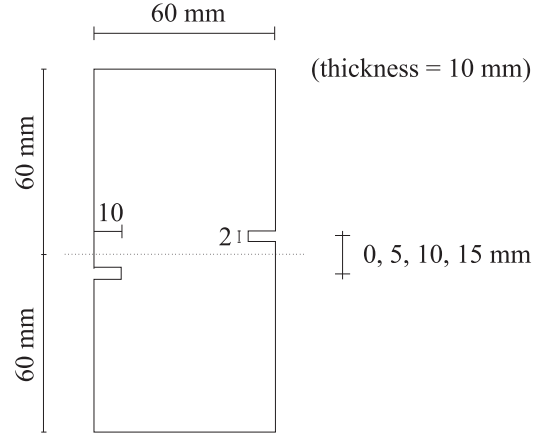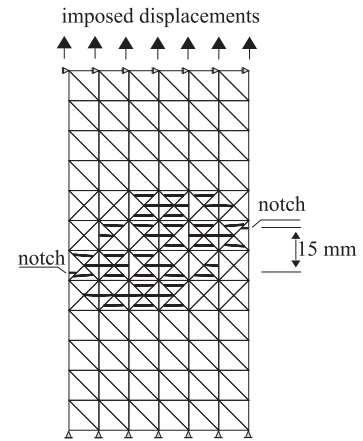

Figure 3: Double-edge notched specimen.

Figure 4: Non-continuous crack path.

load with the average displacement values measured at the top of the specimen. The material properties adopted are: Young modulus $E = 24\ GPa$; Poisson's ratio $\nu = 0.2$; tensile strength $f_t = 2.0\ MPa$; fracture energy $G_F = 0.059\ N/mm$. The material model adopted is the pure mode I version of the damage model. In this test a nearly homogeneous stress state is obtained in the central zone between the notches. This is why several cracks tend to initiate simultaneously in the finite element analysis. In fig. 4 the crack pattern obtained in a structured mesh is presented. In this result, which corresponds to the 15 mm notch off-set test, no path continuity is enforced. Since all the discontinuities are forced to evolve through the centroid of the elements, the experimental crack paths can not accurately be reproduced and a chaotic crack pattern is found. In fig. 5a, the same mesh is used but path continuity is enforced. In figs. 5b an unstructured mesh is shown. It is interesting to see that, in both cases, the two cracks avoid each other at the centre, as was observed experimentally (Shi et al. 2000).

The same analysis is performed with the 5 mm off-set notch specimen. In fig. 6a the crack pattern obtained with a structured mesh is presented, whereas in fig. 6b the crack pattern obtained with an unstructured mesh is shown. From figs. 6a and 6b it can be
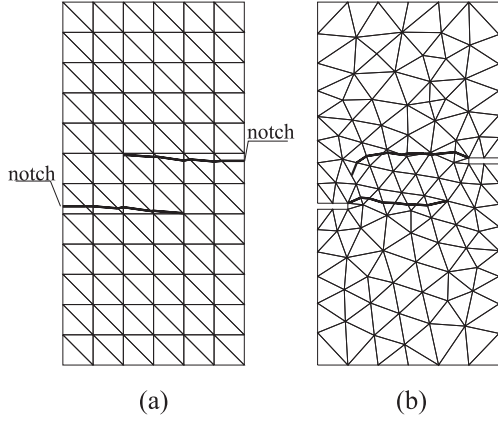
5
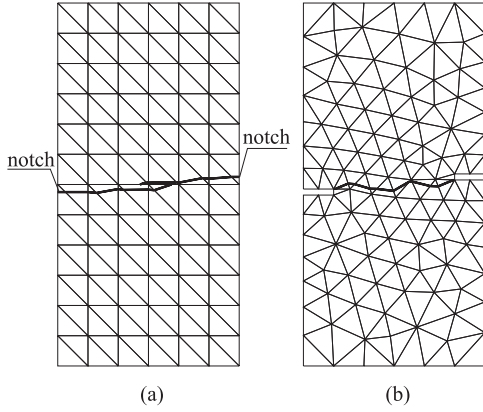
Figure 5: 15 mm offset: continuous crack paths.

Figure 6: 5 mm off-set notches: continuous crack paths.

seen that, unlike the 15 mm test, the two cracks tend to reach each other near the centre, which was also observed experimentally.

In fig. 7 the load displacement curves obtained for the 15 mm test, both experimentally and numerically, are presented.

5.2 SHEAR TESTS

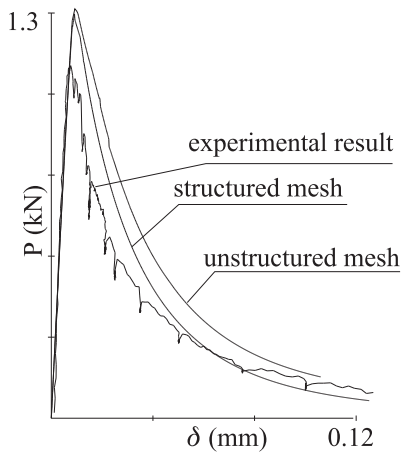The single-edge notched (SEN) beam, experimentally tested by Schlangen (Schlangen 1993; Schlangen and

Figure 7: 15 mm notch off-set: load displacement curves.
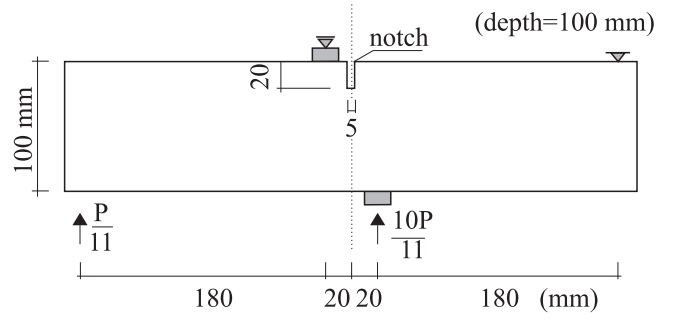
Figure 8: Single-edge notched beam: dimensions and boundary conditions.

van Mier 1993), is analyzed (see fig.8). The arc length method is used to enforce a monotonic increasing of the sliding at the notch (crack mouth sliding displacement, CMSD), which was the control parameter also adopted experimentally. The material properties adopted are (Wells and Sluys 2001): Young modulus $E = 35\ GPa$; Poisson's ratio $\nu = 0.15$; tensile strength $f_t = 2.8\ MPa$; fracture energy $G_F = 0.1\ N/mm$. In these numerical tests the following constitutive models are adopted:

1. a pure mode I model based on the damage model;

2. a mixed mode model based on the damage model; two different tests with this model have been carried out, taking into account different values for the initial shear stiffness:

   (a) $D_{s0} = 100\ N/mm^3$;

   (b) $D_{s0} = 1000\ N/mm^3$.

   In both cases the shear stiffness adopted for an advanced state of damage ($\kappa \gg 0$) is $D_{s\kappa} = 10^{-6}\ N/mm^3$.

3. A mixed mode model based on the plasticity model; two different tests are performed in which the following material parameters for the cohesion (c_0), mode II fracture energy (G_F^{II}), elastic stiffness ($D_{nn}^{el} = D_{ss}^{el}$) and internal friction angle (ϕ) are adopted:

   (a) $c_0 = f_{t0}$; $G_F^{II} = G_F$; $D_{nn}^{el} = D_{ss}^{el} = 10^3\ N/mm^3$; $\tan\phi = 0.75$;

   (b) $c_0 = 2 \times f_{t0}$; $G_F^{II} = 2 \times G_F$; $D_{nn}^{el} = D_{ss}^{el} = 10^3\ N/mm^3$; $\tan\phi = 0.75$;

An unstructured mesh is used (see fig.9). First the mode I model is used. One main crack path is obtained as shown in fig.9. In fig.10 the deformed mesh obtained from the mode I test is presented. As can be seen from fig. 9, the enforcement of crack path continuity results in a curved crack such as the one found experimentally (Schlangen and van Mier 1993). In
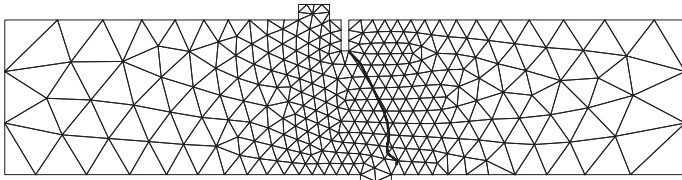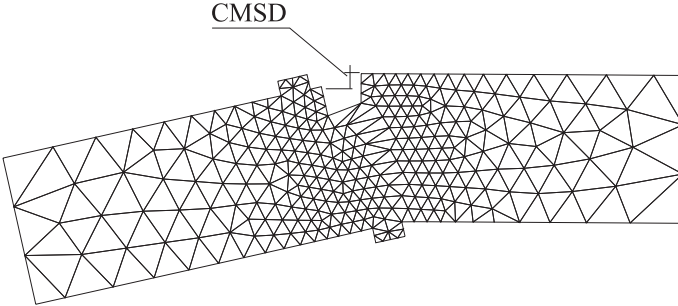
6

Figure 9: Mode I - single crack path.

Figure 10: Deformed mesh.

fig. 11 the load-displacement (P-CMSD) curves obtained with both the damage (solid lines) and the plasticity models (dashed lines) are presented. In these figures the experimental result from (Schlangen 1993) is also shown in bold. From the observation of fig. 11 two main conclusions can be drawn:

1. the experimental peak load is slightly smaller than the numerical peak loads;

2. the experimental response is more ductile than the numerical response.

Regarding the descending branches of the load-CMSD curve, the differences found are related to the modelling of the shear tractions in the fictitious cracks. As already concluded in Alfaiate and Pires
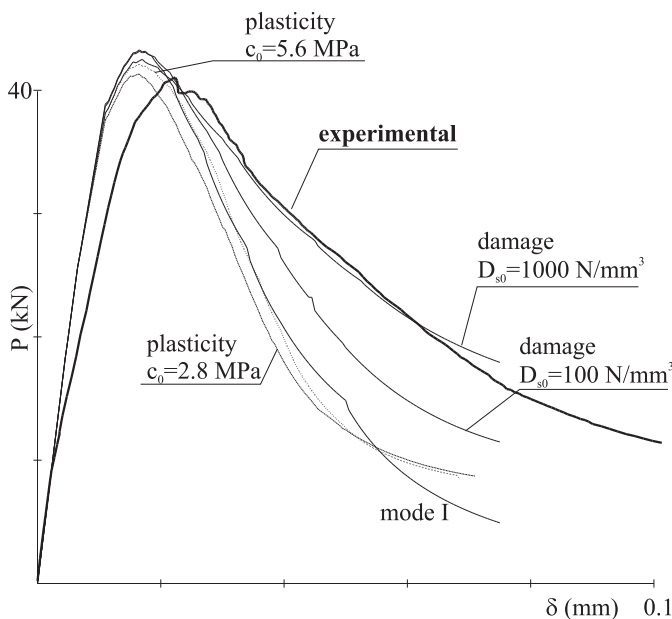

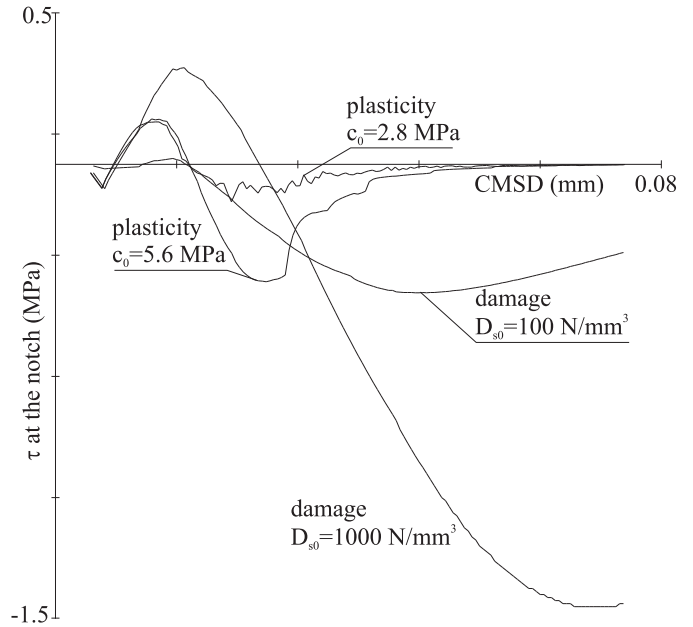Figure 11: Load CMSD curves obtained with mode I model.

Figure 12: Shear tractions at the notch.

(1999), if higher values of the shear tractions are allowed in the fictitious cracks, the more ductile the descending branch becomes. In order to clarify this observation, in fig. 12 the evolution of the shear tractions (τ) at the fictitious crack which first opens, i.e., at the notch, is plotted against the crack mouth sliding displacement CMSD. From fig. 11 it can be concluded that the non-isotropic damage model, which allows for the increase of the shear tractions during the softening behaviour, leads to a more ductile softening branch, which is closer to the experimental curve. A similar conclusion was also drawn in Alfaiate and Pires (1999), where a discrete approach was adopted. As can be seen from fig. 12, the shear tractions τ obtained with the plasticity model are always small during the analysis. Nevertheless, the greatest values of the shear tractions are found with the damage model, for which the shear tractions tend to decrease only after a value of the CMSD close to 0.1 *mm* is reached. The peak loads numerically obtained also depend on the softening criterion adopted: the smallest values are found with the the plasticity model, whereas the highest values are obtained with the damage model. This is due to the fact that both the normal and sliding jump components at the discontinuity are taken into account in the softening law of the plasticity model (see equation (13)), whereas, in the non-isotropic damage model, only the normal jump component is considered (see equation (4)). As a consequence, softening increases faster with the plasticity model than with the damage model, which explains the differences found in the peak loads (Alfaiate et al. 2001).

6 CONCLUSIONS

Embedded strong discontinuities are used to model discrete cracking in materials like concrete. An algorithm is introduced to enforce the continuity of the crack path, permitting a clear identification of the discontinuities in the mesh. First, double-edge notched specimens are analyzed under tension. The influence of the notch offset on the crack patterns is studied. Both structured and unstructured meshes are used. With the enforcement of crack path continuity, it is found that two cracks, each initiating at a different notch, develop towards the centre of the specimen. Depending on the notch offset, these cracks either meet or avoid each other, as observed experimentally. Next, a single-edge notched (SEN) beam is analyzed. Both mode I and mixed mode cracking have been considered in order to assess the importance of the shear tractions on the global behaviour of the structure. It is found that, if higher values of the shear tractions are allowed at the fictitious cracks, the more ductile the descending branch of the load-displacement curve becomes. However, in the examples studied, the shear tractions do not significantly influence the peak load. Instead, the peak load depends on the type of criterion adopted for the evolution of softening: it is verified that the isotropic softening criterion, adopted in the plasticity model, leads to a smaller peak load than the non-isotropic softening criterion used in the damage model. Finally, as general conclusions, it is found that:

1) the results obtained do not depend on the mesh, neither from the size nor from the orientation of the finite elements;

2) crack path continuity allows for the formation of realistic crack patterns similar to those found in experiments, even if reasonably coarse meshes are used and

3) the formulation adopted allows for the correct dissipation of energy leading to he formation of a mechanism in all the examples studied.

Acknowledgements

REFERENCES

Alfaiate, J. and E. B. Pires (1999). Mixed mode fracture in concrete. In F. Aliabadi (Ed.), *International Conference on Fracture and Damage Mechanics*, London, United Kingdom. University of London, Queen Mary & Westfield College London.

Alfaiate, J., E. B. Pires, and J. A. C. Martins (1997). A finite element analysis of non-prescribed crack propagation in concrete. *Computers and Structures 63*(1), 17–26.

Alfaiate, J., G. N. Wells, and L. J. Sluys (2001). On the use of embedded discontinuity elements with crack path continuity for mode i and mixed mode fracture. submitted.

Armero, F. and K. Garikipati (1996). An analysis of strong discontinuities in multiplicative finite strain plasticity and their relation with the numerical simulation of strain localization. *International Journal of Solids and Structures 33*(20–22), 2863–2885.

Carpinteri, A., S. Valente, and P. Bocca (1989). Mixed mode choesive crack propagation. In K. Salama, K. Ravi-Chandar, D. Taplin, and P. R. Rao (Eds.), *7th Int. Conf. on Fracture (ICF-7)*, New York, USA, pp. 2243–2257. Pergamon Press.

Oliver, J., M. Cervera, and O. Manzoli (1999). Strong discontinuities and continuum plasticity models: the strong discontinuity approach. *International Journal of Plasticity 15*(3), 319–351.

Schlangen, E. (1993). *Experimental and numerical analysis of fracture processes in concrete*. Ph. D. thesis, Delft University of Technology.

Schlangen, E. and J. G. van Mier (1993). Mixed-mode fracture propagation: a combined numerical and experimental study. *Fracture and damage of concrete and rock*, 166–175.

Shi, C., A. G. van Dam, J. G. M. van Mier, and L. J. Sluys (2000). Crack interaction in concrete. In F. H. Wittmann (Ed.), *Materials for Buildings and Structures EUROMAT*, Volume 6, pp. 125–131. Weinheim, Germany: WILEY-VCH Verlag.

Wells, G. N. and L. J. Sluys (2001). Three–dimensional embedded discontinuity model for brittle fracture. *International Journal of Solids and Structures 38*(5), 897–913.